PNAS
www.pnas.org

Supplementary Information for

Cats use hollow papillae to wick saliva into fur

Alexis C. Noel and David L. Hu

David L. Hu
E-mail: hu@me.gatech.edu

This PDF file includes:

Supplementary text
Figs. S1 to S4
Tables S1 to S4
Captions for Movies S1 to S4
References for SI reference citations

Other supplementary materials for this manuscript include the following:

Movies S1 to S4

Supporting Information Text

Experimental methods

High speed videography, kinematics, and forces during grooming. Using high-speed camera equipment, a Phantom Miro M110 at 500 frames per second, we filmed an adult short-haired domestic cat at the Georgia Institute of Technology. To observe grooming kinematics of the domestic cat, we wiped a a wet washcloth on the back of the cat to entice it to groom. The fur was lit with LED lighting. The ensuing videos were tracked by hand using Tracker software to determine tongue kinematics.

Nylon fur (Mongolian 60 inch faux ivory fur with hair length of 8 cm) was procured from thefabricexchange.com, and secured to a force plate (AMTI HE6x6). The fur was sprayed with a pheromone-based calming fluid (Feliway) to entice the cats to lick the fur. Filming by a video camera (high-definition Sony HDR-HC9) served to synchronize grooming motions to force measurements. We measured the force applied by the tongue to the force plate, and found that the cat pressed down with 0.13 ± 0.13 N of force (average for 29 lick measurements from a single cat). A sample of grooming forces normal (F_z) and parallel (F_x) to the plate during a grooming trial is shown in Figure S1.

Tongue and papilla μCT visualization. Cat tongues were procured from the following sources: six domestic cat tongues from the Applied Physiology department at Georgia Tech; one tiger tongue from Zoo Atlanta; three bobcat tongues and one cougar tongue from Carter Taxidermy; three tiger tongues, one snow leopard tongue, and one lion tongue from the Department of Small Animal Clinical Services at University of Tennessee and Tiger Haven. We first measured tongue dimensions by hand and report these values in Table S2. The lengths L_T and widths W_T of the cavo papillae region have scalings of $L_T \sim M^{0.42}$, $W_T \sim M^{0.42}$, where M is body mass. Thus the grooming region scales nearly as expected based on isometry, the assumption that the tongue's proportion does not change with body size.

We first used a Scanco μCT50 x-ray micro-computed tomography machine to scan an entire domestic cat tongue. A cat tongue was collected post-mortem, severed at the attachment with the throat. We placed the tongue in a 30-mm diameter tube, and scanned at a voltage of 45 kVp and current of 200 μA.

To visualize the papillae, we removed the largest grooming papilla from each cat tongue using a scalpel and tweezers from the region shown in Figure 2**D**. During this process, the tongue was still frozen. We removed tissue remnants from the base cavity of the papilla using tweezers, and rinsed the papilla in water. Care was taken to avoid compressing the papillae with the tweezers. Each cat papilla was placed into a 3 mm diameter tube and scanned at highest resolution with 45 kVp and 200 μA. We measured the cavity width, height, and volume from the scan using Blender software, and tabulate the data in Table S3.

Measuring cat fur properties. We measured the dimensions of fur for 6 cat species (cheetah *Acinonyx jubatus*, caracal *Caracal caracal*, Caucasian wildcat *Felis sylvestris caucasica*, leopard *Panthera pardus*, snow leopard *Panthera uncia*, and tiger *Panthera tigris*) at the Museum of Comparative Zoology at Harvard University. We further measured fur samples of 3 other species (bobcat *Lynx rufus*, cougar *Puma concolor*, and Eurasian lynx *Lynx lynx*) from furs procured from Promise Land Tannery. Using a portable Andonstar A1 USB microscope, we measured diameter and length of down hairs. Additional fur density and length values were gathered from literature (1–3). Fur density values from literature included both down and guard hairs - in our model, we assume this density value as an approximation for down hair density. While fur density and length may vary across the cat body, we only compare values measured at the midpoint of the cat back to remain consistent with literature. Hair and fur properties with associated references are tabulated in Table S4.

Measurement of fluid transferred from cat grooming. We designed and constructed a "grooming machine" that is able to pull a tongue across a sample of fur (Figure S2). An encoded motor (12V 25D mm gearmotor from Pololu.com), controlled by an Arduino microcontroller, drives a rack-and-pinion horizontally. The machine is able to vary pulling speeds. The tongue is secured to the end of the rack-and-pinion. To measure grooming forces, we used an AMTI HE6x6 force plate, with 2.2 N capacity in the X and Y direction, and 4.4 N capacity in the Z direction (into the plate).

We determined the amount of fluid transferred during a single grooming lick by weighing a wetted tongue before and after a groom. Before the experiment, we dried the tongue using paper towels and a hair dryer, and weighed the tongue using a Mettler Toledo analytical balance. The tongue's carrying capacity for water was found by dipping a dry tongue in water, letting the excess fluid drip off, then weighing the wetted tongue. We repeated this process for only the dorsal and posterior side of the tongue. The dorsal side of the tongue, used in grooming , can hold 0.12 μL of water total, 1.3 times more than the smooth back of the tongue. The fluid in the papillae cavities accounts for 5% of total fluid on the top of the tongue.

To simulate a grooming lick, we secured the severed cat tongue to the end of the rack-and-pinion of the grooming machine. We procured a sample of the same cat's fur, of length L_{groom}. This fur was secured to the AMTI HE6x6 force plate. During a trial, the tongue was pulled through the fur sample at speed v_{groom}. The spacing between tongue and fur was adjusted so that the tongue applies a constant normal force of 0.1 N, approximating the measured grooming forces.

In Figure 4**E**, we report the volumes of water transferred after substracting the artifacts due to evaporation, as shown in Figure S3 of the Supplement. To measure the rate of water evaporation from the cat tongue surface, we first dried a severed cat tongue using towels and a hair dryer, then measure the tissue mass using a Mettler Toledo analytical balance. Next, we dipped a severed tongue in water, allow it to drip, and then weighed the wetted tissue over a period of 80 seconds. The difference in wet and dry tissue mass provides the evaporative water loss over time. We find that approximately $V_e = 6$ microliters of water evaporates from the tongue surface over a 30 second period, the length of a single trial. For visualization, we repeated the above experiment using cat's tongue, dyed with food coloring, and nylon fur, shown in Figure 4**C-D**.

Grooming forces with the TIGR Brush. Using the TIGR Brush with the grooming machine, we measured grooming forces with a faux fur sample. The faux nylon fur, Mongolian 60 inch faux fur ivory with hair length of 8 cm, is the same material from the grooming force measurements. To simulate tangled fur, we blew air over the sample using a hair dryer for 30 seconds; the long lengths of the fur naturally caused it to tangle when blown. We pulled the TIGR Brush through the fur 7 times and measured the force along the grooming direction; between each trial, the mimic was reset and the fur was left untouched. We repeated the experiment with a human hairbrush for comparison [Figure 5**B**]. The hairbrush, a Conair cushion brush with plastic bristles, was altered for testing: the flexible base with bristles was detached from the brush handle, secured to a 3D printed mount using epoxy, and the bristles were tripped to a height of 9 mm, the same height as the papillae mimic. The TIGR Brush and Conair hairbrush were attached to the rack-and-pinion identically. For both brushes, the spacing between fur and brush was set to that compressive force into the fur was 0.1 N, identical to a real grooming scenario.

Materials characterization methods

Young's modulus of tissue and papilla. We measured the softness of the domestic cat tongue using micro-indentation. A domestic cat tongue was collected from Georgia Institute of Technology and tested within 10 hours of death. The tongue was severed at the base connection to the throat. We used a TA Instruments ElectroForce 3100 to perform probe indentation tests on the cat tongue. We used a rigid, flat-ended cylindrical indenter of diameter 2 mm to probe the soft tissue on the underside of the tongue, where there are no papillae. Within the linear elastic solid regime, the Young's modulus is determined using:

$$F = \frac{2E_{\text{tongue}} r\delta}{1-\nu^2} \qquad [1]$$

where E_{tongue} is the tongue's Young's modulus, r is the indenter radius, δ is displacement, and ν is the Poisson's ratio. Poisson's ratio is assumed to be 0.5 for a perfectly elastic material (4). The Young's modulus was calculated from the force and displacement measured from the indenter. The average Young's modulus of the cat tongue is 9.1 ± 3.7 kPa (N = 5 trials from a single cat tongue). The softness value correlates well to the Young's modulus of muscle at 7 kPa (5). Next, we removed a single papillae from the cat tongue tissue and the tested Young's modulus in a nanoindenter (Hysitron TriboIndenter). The Young's modulus of the papillae is 1.66 - 1.94 GPa ± 3%, similar to human fingernails (6). The error from the nanoindenter originates from the control measurements of polycarbonate samples immediately before and after the papillae testing, providing correct modulus values within ± 3%.

Math methods

Fluid wicking in the papillae. We used three cat papillae (from one domestic cat and two tigers) to demonstrate the high rate of wicking. Using the same camera and lighting in the cat grooming experiments, we filmed the motion of the fluid front in the papillae. In Figure 2**F**, the solid squares show wicking into a domestic cat papilla, with a power law of $z \sim t^{0.65}$ (R^2=0.97), where t is time. Solid and open triangles show wicking into two separate tiger papilla with power laws of $z \sim t^{0.56}$ (R^2=0.98) and $z \sim t^{0.57}$ (R^2=0.97) respectively.

The exponents for these trends is close to 1/2, consistent with Washburn's Law for capillary flow in a half-pipe of radius r (identical to a capillary tube), where flow is resisted by viscous forces. Washburn's Law (7) states that the position of the fluid front $z = (\frac{\sigma r \cos(\theta_p)}{2\mu})^{1/2} t^{1/2}$, where θ_p is the fluid contact angle, and μ is the fluid viscosity. Using the contact angle θ_p as a free parameter in Washburn's Law yields the red line in Figure 2**F**, which fits the data well. Moreover, we predict that the contact angle of water on the three papillae is $89.9° \pm 0.15°$(N=3). This contact angle suggests that papillae are mildly hydrophilic. Indeed, Supp. video S3 shows a precursor film spreading ahead of the fluid front, which makes the cavity hydrophilic.

Water wicked into a papilla remains stable. This observation is consistent with the value of the Bond number (8), which describes the magnitude of the gravitational forces compared to surface tension. The Bond number may be written $Bo = \frac{\rho g {w_{\text{cavity}}}^2}{\sigma} = 0.012 \ll 1$, where w_{cavity} is the papilla cavity width, g is gravitational acceleration, and ρ is the density of water and and σ is the surface tension of water. Since the Bond number is small, the fluid in the papilla remains stable due to the forces of surface tension.

Mathematical model for fur height. The porosity of fur, or the fraction of air in a given volume of fur, is given by

$$\epsilon = \frac{V_{\text{air}}}{V_{\text{total}}} = \frac{V_{\text{total}} - V_{\text{hairs}}}{V_{\text{total}}}, \qquad [2]$$

where V_{air} and V_{hairs} are the volumes of air and hair in a given volume V_{total}. We simplify 2 by considering a rectangular prism of fur, with fur height h_{fur}, and width and length of the tongue W_{T}, and L_{T} as shown in the red dotted box in Figure 3**A**. The air volume V_{air} can be written as the total volume V_{total} minus the volume V_{hairs} of all hairs in this region. Each down hair is cylindrical with a radius r_{hair} and length L_{hair}. The total hair volume is the product of the volume of each hair $\pi r_{\text{hair}}^2 L_{\text{hair}}$, and the number of hairs, which can be written as the hair density per unit area, ρ_{fur}, multiplied by the area $W_{\text{T}} L_{\text{T}}$. Thus, 2 simplifies to:

$$\epsilon = \frac{h_{\text{fur}} W_{\text{T}} L_{\text{T}} - \rho_{\text{fur}} W_{\text{T}} L_{\text{T}} \pi r_{\text{hair}}^2 L_{\text{hair}}}{h_{\text{fur}} W_{\text{T}} L_{\text{T}}}. \qquad [3]$$

Simplifying and rearranging 3 enables us to write the fur depth h_{fur}, defined as the distance between the skin and tongue, as:

$$h_{\text{fur}} = \frac{\rho_{\text{fur}} \pi r_{\text{hair}}^2 L_{\text{hair}}}{1 - \epsilon}. \quad [4]$$

4 states that the more the hair is compressed, the lower the porosity. We can take 4 to its very limits by considering the maximum compression of fur. The closest the cylindrical hairs can pack together is in a hexagonal packing arrangement (9), resulting in the lowest attainable porosity of

$$\epsilon_{min} = 1 - \frac{\pi\sqrt{3}}{6} = 0.093. \quad [5]$$

We use this value of the minimum porosity to determine the minimum compressed height of fur, when all hairs lay parallel to the skin.

Wicking through porous fur. We apply Darcy's model for wicking in porous media (10) to determine the volume and depth of saliva wicked into the fur. The tongue is idealized as an infinite reservoir of fluid. In reality, the dorsal side of the tongue can only hold a maximum of 0.12 mL of water, or 2.4 eyedropper drops, and therefore our analysis is only valid for volumes wicked below this amount. When the tongue is contact with the fur, the depth to which saliva can penetrate may be written

$$h_{\text{saliva}} = \left(\frac{4K\sigma\cos(\theta_h)}{\epsilon\mu R_{\text{p}}} \right)^{1/2} t^{1/2}, \quad [6]$$

where K is permeability, R_{p} is the mean pore radius of the fur, θ_h is the contact angle of saliva on hair, μ is the saliva viscsoity, and t is the time that the tongue remains in contact with the fur. We assume that saliva is flowing in the transverse direction through an array of cylindrical hairs as shown in Figure 4**B**.

The mean pore radius across a bank of constant-radius fibers may be written (11): $R_{\text{p}} = 2r_{\text{hair}} \frac{\epsilon}{1-\epsilon}$. The permeability K of the porous media is determined using the Carman-Kozeny equation for transverse flow through cylindrical fibers (12): $K = \frac{{r_{\text{hair}}}^2}{4k} \frac{\epsilon^3}{(1-\epsilon)^2}$, where k is the Kozeny constant, equal to 10 for transverse flow. Fur is an example of a dynamic porous media because the mean pore radius will change as fluid is introduced. This is due to the fact that hairs bend when surface tension forces are applied. As analyzed by Py and Boudaoud (13), wet fibers aggregate into bundles, where the porosity of these bundles is considered to be close-packed hexagonal packing. Therefore, hairs will form bundles when wetted [Figure 4**A**], decreasing porosity to its lowest attainable value [Figure 4**B**]. Thus, in our analysis, we use a wetted fur porosity of $\epsilon = \epsilon_{\text{min}} = 0.093$.

As shown by 6, the saliva can penetrate deeper the longer the tongue remains in contact with the fur. For grooming, the contact time $t \sim \frac{L_{\text{T}}}{v_{\text{groom}}}$ scales as the ratio of tongue length to grooming velocity v_{groom}. We substitute this contact time into 6 to estimate the depth the saliva has seeped. Saliva will fill the air pockets between hairs; therefore, the volume V_{fluid} of saliva wicked into the fur is:

$$V_{\text{fluid}} = \epsilon h_{\text{saliva}} W_{\text{T}} L_{\text{groom}}, \quad [7]$$

where L_{groom} is the lick length of the groom. By substituting h_{saliva} from 6 into 7, the volume of saliva may be written

$$V_{\text{fluid}} = \left(\frac{\sigma\cos\theta_h}{\mu} \right)^{1/2} \left(r_{\text{hair}} L_{\text{T}} W_{\text{T}}^2 \right)^{1/2} \left(\frac{L_{\text{groom}}^2}{v_{\text{groom}}} \right)^{1/2} \left(\frac{\epsilon^3}{20\,(1-\epsilon)} \right)^{1/2}. \quad [8]$$

8 consists of four types of inputs, including saliva properties, fur and tongue geometry, grooming kinematics, and fur porosity. Values for these inputs are measured from experiments and reported in Tables S1-S4 of the Supplement. We use water as a substitute for cat saliva, with the contact angle of water on hair of (14) $\theta_h = 60°$, and $\mu = 8.9 * 10^{-4}$ Pa·s is the viscosity of water.

In our model, we assume that saliva will act like water. In actuality, saliva is a non-Newtonian shear-thinning fluid, with viscosity changing based on applied shear rate. We can show that this assumption is within reason by analyzing the shear rate of fluid passing through the hairs. The shear rate $\dot{\gamma}$ of fluid passing through a pore is a function of flow velocity and a length scale: $\dot{\gamma} = v_{\text{wick}}/R_{\text{p}}$, where $v_{\text{wick}} = h_{\text{saliva}}/t$ is the steady state wicking speed and R_{p} is the pore radius at minimum porosity. We find $\dot{\gamma} > 10^6 \text{s}^{-1}$; therefore, assuming cat saliva has similar shear-thinning properties as human saliva (15), viscosity will be $\mu_{\text{saliva}} \approx 10^{-3}$ Pa·s, on par with the viscosity of water $\mu_{\text{water}} = 0.89 \times 10^{-3}$ Pa·s.

Table S1. Grooming kinematics for 8 cats

Species	N	Trials	L_{groom} (mm)	v_{groom} (mm/s)	Ref.
Cat (*Felis catus*)	3	5	63 ± 20	220 ± 9.3	Measured
Bobcat (*Lynx rufus*)	3	8	38 ± 18	150 ± 1.2	YouTube (Benji The Bobcat)
Cougar (*Puma concolor*)	1	1	120	270	YouTube (Mexicrackah)
Snow leopard (*Panthera uncia*)	1	3	53 ± 27	220 ± 19	YouTube (TheSacramentoZoo)
Tiger (*Panthera tigris*)	3	8	190 ± 36	270 ± 20	YouTube (IEAS, BigCatDerek)
Lion (*Panthera leo*)	1	4	180 ± 57	260 ± 38	YouTube (Stoney Edwards)
Leopard (*Panthera pardus*)	1	5	79 ± 3	240 ± 18	YouTube (Lock Head)
Black Panther (*Panthera pardus*)	1	2	74 ± 10	270 ± 38	YouTube (Lock Head)

Table S2. Tongue properties for 6 species of cat

Species	Sex	Tongue samples	M (kg)	L_{T} (mm)	W_{T} (mm)
Cat (*Felis catus*)	F	2	4	16.5 ± 3.5	13.0 ± 2.8
Bobcat (*Lynx rufus*)	2F, 1M, 1 unknown	4	10.5 ± 1.6	23.5 ± 3.1	21.3 ± 1.7
Cougar (*Puma concolor*)	F	1	54	38.0	33.0
Snow leopard (*Panthera uncia*)	M	1	40	42.0	33.0
Tiger (*Panthera tigris*)	F	4	116.3 ± 25.6	64.0 ± 11.3	54.5 ± 4.4
Lion (*Panthera leo*)	F	1	135	71.0	60.0

Table S3. Cavo papillae properties for 6 species of cat

Species	h_{papillae} (mm)	w_{cavity} (mm)	V_{cavity} (μL)
Cat (*Felis catus*)	2.1	0.30	0.014
Bobcat (*Lynx rufus*)	2.3	0.30	0.009
Cougar (*Puma concolor*)	2	0.30	0.035
Snow leopard (*Panthera uncia*)	2.3	0.17	0.021
Tiger (*Panthera tigris*)	2.3	0.22	0.082
Lion (*Panthera leo*)	2.7	0.50	0.160

Table S4. Down hair and fur properties for 19 cats

Species	M (kg)	r_{hair} (μm)	ρ_{fur} (hairs/mm^2)	L_{hair} (mm)	Ref.
Caucasian wildcat (*Felis silvestris caucasica*)	5	9.5	80	35	Measured, (2)
Caracal (*Caracal caracal*)	11.8	9.6	25	30	Measured, (2)
Eurasian lynx (*Lynx lynx*)	18	9.3	90	35	Measured, (2)
Cheetah (*Acinonyx jubatus*)	40	14.5	20	25	Measured, (2)
Snow leopard (*Panthera uncia*)	32	9.2	40	50	Measured, (2)
Leopard (*Panthera pardus*)	27	10.2	30	30	Measured, (2)
Tiger (*Panthera tigris*)	130	15.0	25	30	Measured, (2)
Bobcat (*Lynx rufus*)	8.6	7.9	90	31	Measured
Cougar (*Puma concolor*)	54	8.9	80	35	Measured
American short hair (*Felis catus*)	4	11.0	75	37	Measured, (3)
Siamese (*Felis catus*)	4	11.0	75	28	(3)
Egyptian Mau (*Felis catus*)	4	11.0	75	31	(3)
Oriental short hair (*Felis catus*)	4	11.0	75	35	(3)
Himalayan (Persian) (*Felis catus*)	4	11.0	75	50	(3)
Japanese cat (Native) (*Felis catus*)	4	11.0	75	58	(3)
Persian (*Felis catus*)	4	11.0	75	81	(3)
Chincilla (Persian) (*Felis catus*)	4	11.0	75	88	(3)
English rex (*Felis catus*)	4	8.1	75	20.4	(1)
German rex (*Felis catus*)	4	8.5	75	20.6	(1)

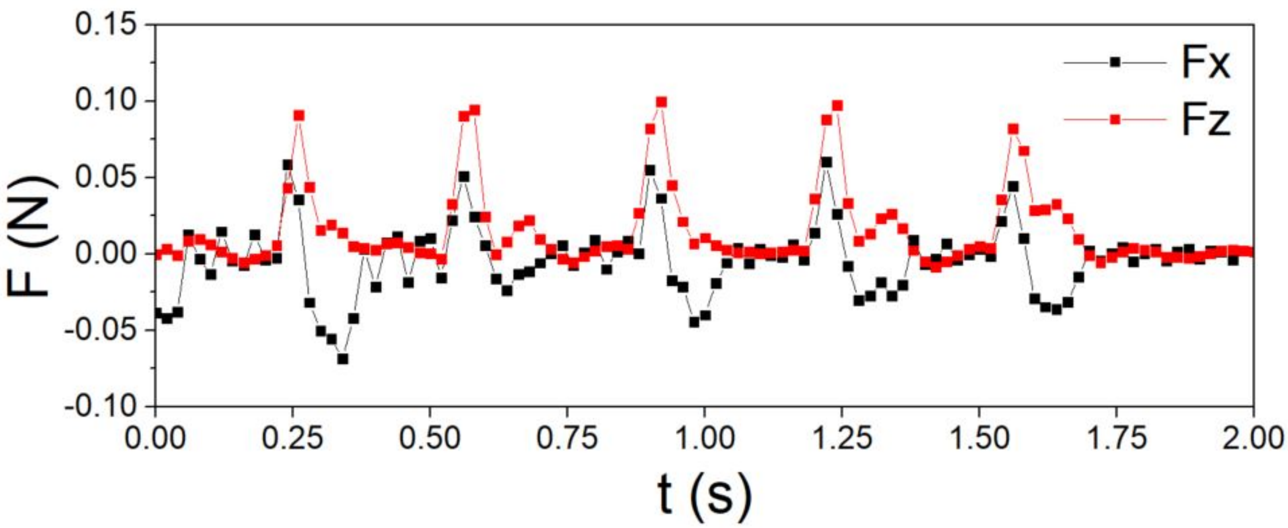

Fig. S1. Normal (F_z) and parallel (F_x) forces exerted by a domestic cat tongue during a grooming trial.

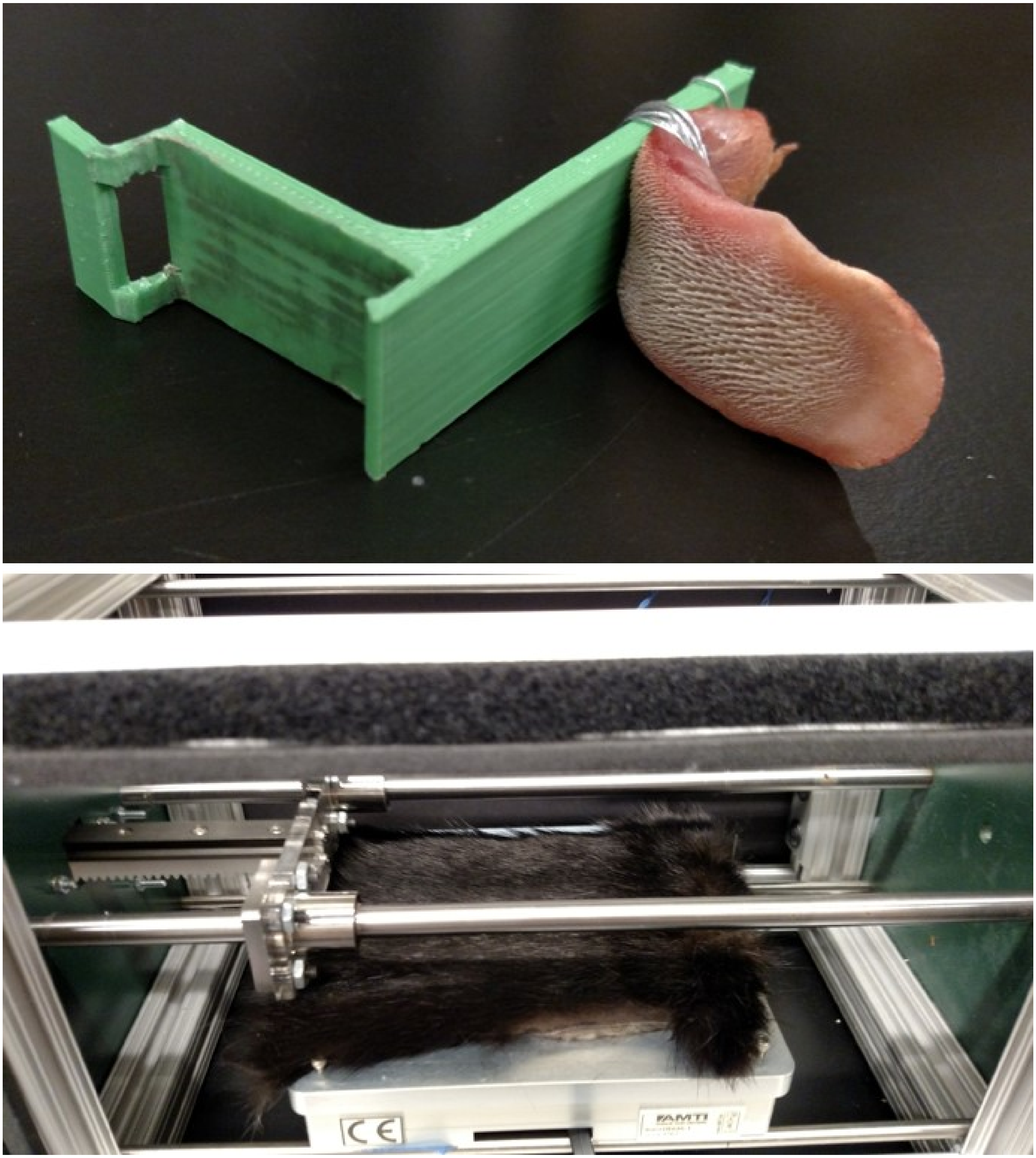

Fig. S2. Grooming machine. A cat tongue (top) is driven through a sample of cat fur (bottom) at a fixed velocity and fixed normal force of 0.1 N as measured by the AMTI HE6x6 force plate. The TIGR Brush and human hairbrush are also tested with the grooming machine.

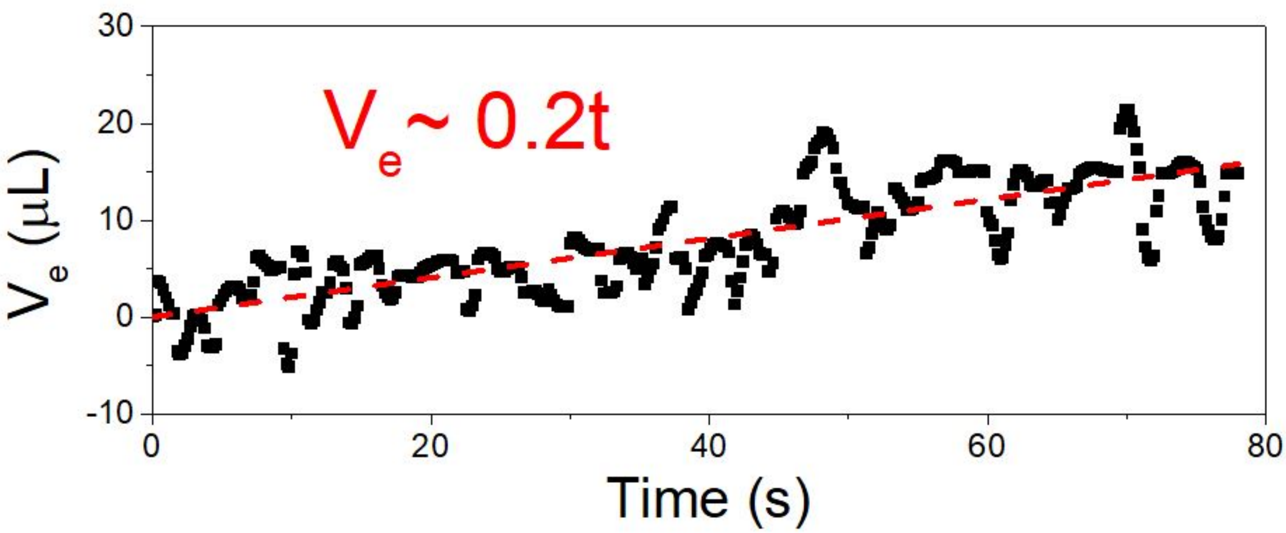

Fig. S3. Volume of water V_e evaporated from tongue surface over time; 6 μL of water evaporates over 30 seconds.

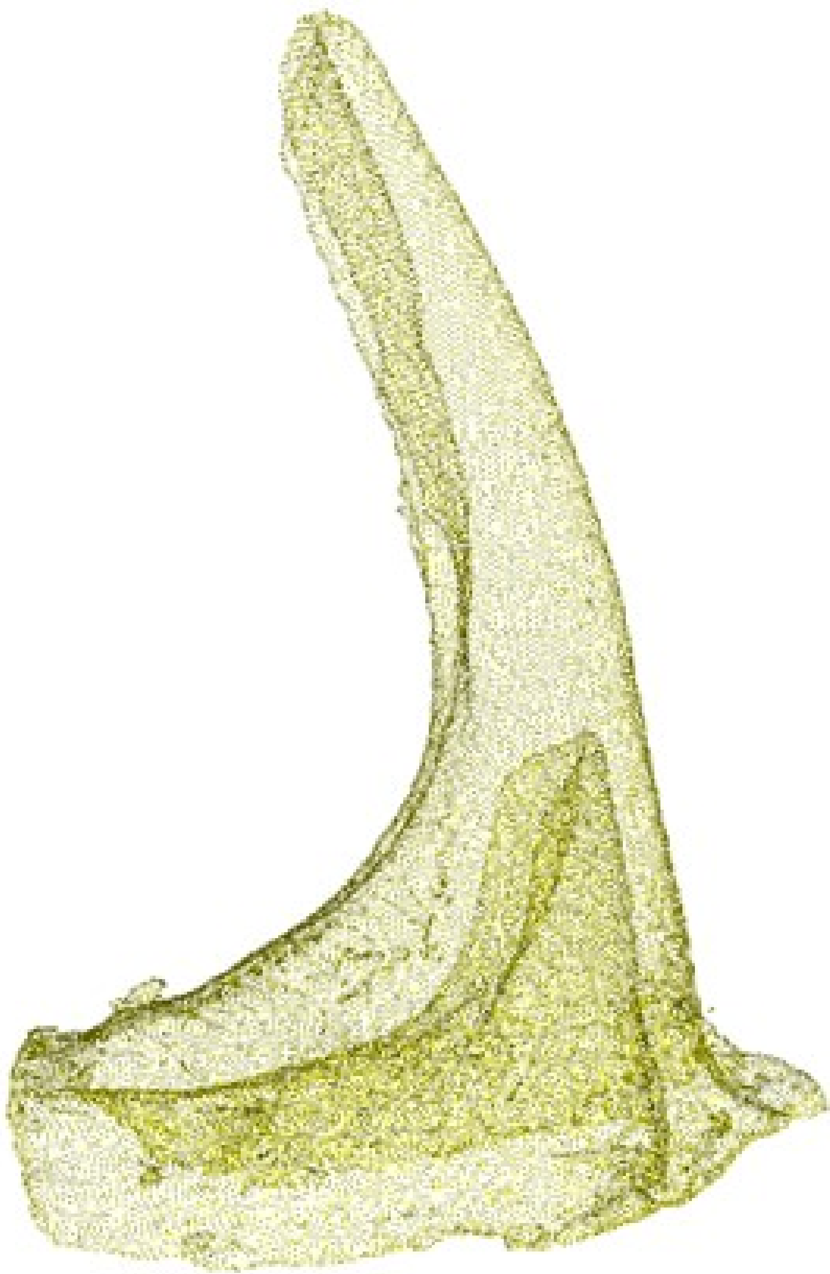

Fig. S4. A transparent model of a domestic cat's papilla, illustrating cavities present.

Movie S1. Cavo papillae of a domestic cat rotating perpendicular to tongue during grooming filmed at 1000 fps, slowed 25x.

Movie S2. Cat grooming videos, in order: cat, bobcat, cougar, snow leopard, tiger, lion, and leopard and black panther. Video credits in order: Alexis Noel, YouTube contributors Benji The Bobcat, 5831a, Mexicrackah, Stoney Edwards, Dougie Hamilton, and TheSacramentoZoo.

Movie S3. Tiger papilla wicking orange food dye. A precursor film can be seen advancing before the bulk fluid motion.

Movie S4. Easy hair removal from 3D-printed cat tongue mimic.

Additional acknowledgements

For donating animal parts, we thank J. Mendelson at Zoo Atlanta, R. Nichols at Georgia Tech, Carter Taxidermy, E. Ramsay and the Pathology Service of the UT College of Veterinary Medicine, and Tiger Haven. We thank C. Hobbs for photography, A. Lin for μ-CT scanning, The Museum of Comparative Zoology at Harvard Univ. for fur samples, T.-W. Tsai and K. Kabbabe for early contributions and A-C. Gagnon and G. Marignac at the National Veterinary School of Alfort in France advice. We thank YouTube contributors including Benji The Bobcat, 5831a, Mexicrackah, Stoney Edwards, Dougie Hamilton, and TheSacramentoZoo.

References

1. Searle A, Jude A (1956) The rex type of coat in the domestic cat. *Journal of Genetics* 54(3):506–512.
2. Kitchener AC, Van Valkenburgh B, Yamaguchi N (2010) Felid form and function. *Biology and conservation of wild felids* pp. 83–106.
3. Sato H, Matsuda H, Kubota S, Kawano K (2006) Statistical comparison of dog and cat guard hairs using numerical morphology. *Forensic science international* 158(2):94–103.
4. McKee CT, Last JA, Russell P, Murphy CJ (2011) Indentation versus tensile measurements of young's modulus for soft biological tissues. *Tissue Engineering Part B: Reviews* 17(3):155–164.
5. Engler AJ, Richert L, Wong JY, Picart C, Discher DE (2004) Surface probe measurements of the elasticity of sectioned tissue, thin gels and polyelectrolyte multilayer films: correlations between substrate stiffness and cell adhesion. *Surface Science* 570(1):142–154.
6. Farren L, Shayler S, Ennos A (2004) The fracture properties and mechanical design of human fingernails. *Journal of Experimental Biology* 207(5):735–741.
7. Washburn EW (1921) The dynamics of capillary flow. *Physical review* 17(3):273.
8. Bush JW, Hu DL (2006) Walking on water: biolocomotion at the interface. *Annu. Rev. Fluid Mech.* 38:339–369.
9. Chang HC, Wang LC (2010) A simple proof of thue's theorem on circle packing. *arXiv preprint arXiv:1009.4322*.
10. Masoodi R, Pillai KM, Varanasi PP (2007) Darcy's law-based models for liquid absorption in polymer wicks. *AIChE journal* 53(11):2769–2782.
11. Masoodi R, Pillai KM (2012) A general formula for capillary suction-pressure in porous media. *Journal of Porous Media* 15(8).
12. Lekakou C, Bader M (1998) Mathematical modelling of macro-and micro-infiltration in resin transfer moulding (rtm). *Composites Part A: Applied Science and Manufacturing* 29(1-2):29–37.
13. Py C, Bastien R, Bico J, Roman B, Boudaoud A (2007) 3d aggregation of wet fibers. *EPL (Europhysics Letters)* 77(4):44005.
14. Dickerson AK, Mills ZG, Hu DL (2012) Wet mammals shake at tuned frequencies to dry. *Journal of the Royal Society Interface* p. rsif20120429.
15. Helton KL, Yager P (2007) Interfacial instabilities affect microfluidic extraction of small molecules from non-newtonian fluids. *Lab on a Chip* 7(11):1581–1588.